Photometric investigation of three ultrashort-period contact binaries: Two of them are in special evolutionary stages

L. Liu[1,2,3,4], S.-B. Qian[1,2,3,4], E. Fernández Lajús[5,6], A. Essam[7], M. A. El-Sadek[7] and X. Xiong[1,2,3,4]

ABSTRACT

We carried out high-precision photometric observations of three ultrashort-period eclipsing binaries with 2-meter-class telescopes. The light-curve solutions suggested that all targets had evolved into contact phase. The photometric results are as follows: a) 1SWASP J030749.87−365201.7, $q = 0.439 \pm 0.003$, $f = 0.0 \pm 3.6\,\%$; b) 1SWASP J213252.93−441822.6, $q = 0.560 \pm 0.003$, $f = 14.2 \pm 1.9\,\%$; c) 1SWASP J200059.78+054408.9, $q = 0.436 \pm 0.008$, $f = 58.4 \pm 1.8\,\%$. All of their light curves showed O'Connell effects, which can be modeled by assumed cool spots. The cool spots model is strongly supported by the night-to-night variation of the I-band light curves of 1SWASP J030749.87−365201.7. For a comparing study, we collected all of well-studied ultrashort-period contact binaries (USPCBs) with P < 0.24 day (27 in total), and found that most of them (16 of 27) are shallow contact ($f < 20\,\%$) while only 4 of 27 USPCBs are deep fill-out factors ($f > 50\,\%$). One of the four deep USPCBs is found by this paper. Generally, contact binaries with deep fill-out factors are going to merge. But the USPCBs are believed as they just evolved into contact phase. Hence, the deep USPCB, 1SWASP J200059.78+054408.9, is a contradiction, which makes it

[1]Yunnan Observatories, Chinese Academy of Sciences, 396 Yangfangwang, Guandu District, Kunming, 650216, P. R. China (e-mail: LiuL@ynao.ac.cn)

[2]Key Laboratory for the Structure and Evolution of Celestial Objects, Chinese Academy of Sciences, 396 Yangfangwang, Guandu District, Kunming, 650216, P. R. China

[3]Center for Astronomical Mega-Science, Chinese Academy of Sciences, 20A Datun Road, Chaoyang District, Beijing, 100012, P. R. China

[4]University of Chinese Academy of Sciences, Yuquan Road 19#, Sijingshang Block, 100049 Beijing, China

[5]Facultad de Ciencias Astronómicas y Geofísicas, Universidad Nacional de La Plata, 1900 La Plata, Buenos Aires, Argentina

[6]Instituto de Astrofśica de La Plata (CCT La Plata-CONICET, UNLP), Argentina

[7]National Research Institute of Astronomy and Geophysics, Department of Astronomy, Helwan, Cairo, Egypt

interesting. Particularly, 1SWASP J030749.87−365201.7 is a zero contact binary within a thermal equilibrium, implying that it should be a tune-off sample predicted by the thermal relaxation oscillation (TRO) theory.

Subject headings: binaries : eclipsing – Stars: individuals (1SWASP J030749.87−365201.7, 1SWASP J213252.93−441822.6, 1SWASP J200059.78+054408.9) – Stars: evolution

1. Introduction

The W UMa-type contact binaries are usually composed of two cool main sequence stars where both components are covered by a common convective envelope (CCE). The short-period limit of this type binary is an unquestioned fact. There were some ideals for explaining the limitation: (1) the components become fully convective below a certain period (e.g. Rucinski 1992, 1997; Paczyński et al. 2006; Becker et al. 2011) so that the system becomes unstable; (2) the timescale of the angular momentum loss (AML) is much longer so that the USPCBs cannot be produced under the current age of the universe (Stępień 2006, 2011). Almost fully convective structure makes USPCBs to be different from the F, G and K type contact binaries. Many USPCBs have been found just in recent years with the extraplanet searching projects (One can find the names of the surveys that were introducd by Koen et al. 2016). Norton et al. (2011) published a catalogue of 53 ultrashort-period eclipsing binary (USPEB) candidates, while Lohr et al. (2013a) investigated the period changes of 143 USPEBs, based on the Super Wide Angle Search for Planets (SuperWASP). Koen et al. (2016) confirmed 29 USPEB systems being in overcontact configuration according to a preliminary Fourier decomposition analysis. A series of studies on individual USPCBs have been done in last 5 years (e.g. Dimitrov & Kjurkchieva 2015; Qian et al. 2015a; Liu et al. 2015a; Jiang et al. 2015a). These studies showed that most USPCBs have shallower fill-out factors ($< 20\,\%$). It indicates that USPCBs are in the beginning phase of the contact configuration. And, some USPCBs already have broken the known short-period limitation or low-mass limitation (e.g., SDSS J001641−000925, Davenport et al. 2013; Qian et al. 2015b). The special USPCBs which are under the critical conditions are interesting and important to understand the evolutionary boundary conditions.

For this purpose, and because of the unqualified data of surveys, we observed the USPCB candidates, 1SWASP J030749.87−365201.7, 1SWASP J213252.93−441822.6 and 1SWASP J200059.78+0 with 2-meter-class telescopes. The first one was discovered by Norton et al. (2011), while the second and the third one were discovered by Lohr et al. (2013a). The period of these three system are 19584.393 s (0.22667122 day), 19114.669 s (0.22123459 day) and 17771.663 s

(0.20569054 day), respectively (Lohr et al. 2013a). In the literatures, the light curves of these three USPCBs shown very large scatters. So, in this paper, we analyzed these systems with our new observed high-precision multi-colour light curves. We report here that 1SWASP J030749.87−365201.7 and 1SWASP J200059.78+054408.9, a zero contact and a deep contact, are such special samples mentioned above.

2. Observation and data reduction

The two south sky targets were observed by the 2.15 m Jorge Sahade Telescope (JST) in Complejo Astronomico El Leoncito Observatory (CASLEO), San Juan, Argentina. The JST has been equipped a Versarray 2048B CCD camera at the Cassegrain focus (f/8.5) with a binned of 5×5, yielding a field of view of 5×5 arcmin^2. The standard UBVRI filter system was used. 1SWASP J030749.87−365201.7 was observed from November 24 to the December 4 in 2014 with JST, while 1SWASP J213252.93−441822.6 was observed in September 11, 2015. One can find more observational details in Table 1. The JHK magnitudes (from 2MASS catalogue, Cutri et al. 2003) of target, comparison and check stars are listed in Table 2. The observed data were reduced by the IRAF, with the zero and flat corrections. The differential photometry measuring errors of former are about 0.009 mag, while those of the later are about 0.007 mag. The phases of 1SWASP J030749.87−365201.7 were calculated according to the ephemeris of $2456994.77031 + 0^d.22667122 \times E$ while those of 1SWASP J213252.93−441822.6 were computed based on the formula, $2457276.57884 + 0^d.22123459 \times E$, respectively. One can find the corresponding light curves in Fig 1.

The north sky target was observed by the 1.88 m reflector telescope in the Kottamia Observatory, Astronomy Department, National Research Institute of Astronomy and Geophysics (NRIAG), 11421 Helwan, Cairo, Egypt. This telescope has been equipped a EEV CCD 42-40 camera with a format of 2048×2048 pixels, cooled by liquid nitrogen attached on the Newtonian focus of the 1.88 m Kottamia reflector telescope, yielding a field of view of 10×10 arcmin^2. The standard UBVRI filter system was used, too. As the same as the former two, the target, comparison and check stars are listed in Table 2, too. The same data reduction process has been done. The differential photometry measuring errors are about 0.006 mag. The formula of $2457604.37104 + 0^d.20569054 \times E$ was used to yield the light curves plotted in Fig 1, too.

3. Light curves solution

To determine photometric elements and to understand the geometrical structure and evolutionary state of these three USPCBs, we used the latest version of the W-D code (Wilson & Devinney 1971; Wilson 1979, 1990, 2008, 2012; van Hamme & Wilson 2007; Wilson et al. 2010; Wilson & van Hamme 2014) to analyze their multi-colour light curves.

Usually, the effective temperatures are estimated by colours. At the beginning, we estimated the T_1 (effective temperature of the hot component) based on the JHK colour indexes because our targets are in later spectral type (red colour). The corresponding JHK magnitudes (2MASS catalogue, Cutri et al. 2003) are listed in Table 2. The effective temperatures are computed by the method of Worthey & Lee (2011). Then, we applied the q-search method to find an initial q as the input parameter for the W-D code. Such grid method q-searching is just aimed to make the program to converge faster. In other words, the advantage of the q-search method is just for saving computed time. The results of q-search are displayed in Fig 2. The red crosses are the suggested values of q for each system. During the solutions, the bolometric albedo $A_1 = A_2 = 0.5$ (Rucinski 1969) and the values of the gravity-darkening coefficient $g_1 = g_2 = 0.32$ (Lucy 1967) were used, which correspond to the common convective envelope of both components; square root limb-darkening coefficients were used, according to Claret & Gimenez (1990). The adjustable parameters were: the mass ratio q; the orbital inclination i; the potential Ω (because all solution finally converged to mode 3); the mean temperature of star 2, T_2; the monochromatic luminosity of star 1.

However, all light curves showed O'Connell effects (O'Connell 1951). The presence of cool spots on the more massive component can simulate the light curves very well, and it is supported by i) later type stars have deep convective zones so that they have strong magnetic field; ii) fast rotate later type stars should have more stronger magnetic field than normals (Barnes & Collier Cameron 2001; Barnes et al. 2004); iii) the more massive component has a deeper convective zone than the less massive one (Mullan 1975). For the first target, the situations of the cool spots are more complicated, which is supported by its I-band night-to-night variation of light curves (Fig 3). Three cool spots are added to simulate its light curves. One is on the less massive component and two are on the more massive component. 1SWASP J030749.87−365201.7 has so many spots suggest that it has very strong magnetic activities. Emphatically, the longitudes of spots can be limited exactly by the distortions in the light curves. The other three parameters, latitudes, radii and temperature ratios, however, are not independent. A very recent study of cool spots on M dwarfs revealed that the fractus cool spots occurred on the high latitudes with high frequency (Barnes et al. 2015), according to the doppler maps. Although our cool spots model is a probably result, the differential of results with and without cool spots is usually less than 10% (e.g. Qian et

al. 2011, 2013a).

Finally, the light curve solutions are listed in Table 3, and the elements of the assumptive cool spots are listed in Table 4. The corresponding fittings of each light curve are shown in Fig 1, while the residuals of the fittings are shown in Fig 4. The differential colours diagrams are shown in Fig 5. In this figure, it is clearly seen that colours of the systems varied with the phases, like their light curves. And there is a swell in colour curves of 1SWASP J030749.87−365201.7 around the phase of 0.40. The swell means a higher temperature. The amplitude of the colour curves suggest an uncertainty of 700 K for the temperature estimation, but it do not change any uncertainty of the temperature ratio (T_1/T_2). At last, the geometric constructions of the three USPCBs and the present cool spots are displayed in Fig 6.

4. Discussion of the solutions

In this section, we will mainly discuss about the reliability of the photometric solutions and the evolutionary states revealed by the solutions. The resolved inclinations of these three systems are greater than 75 degree, strongly indicating that their photometric mass ratios are similar to their spectroscopic mass ratios (Maceroni & van't Veer 1996). Hence, the photometric mass ratios of our solution should be acceptable. The solutions show that these three systems are in contact phase, with moderate mass ratios. However, 1SWASP J200059.78+054408.9, with the shortest period among the three, have a deep contact factor of 58.4 %. Deep USPCBs are very few. It is supported both by the observational facts and by the theory. 27 well-studied USPCBs (P $<$ 0.24 day) are collected in Table 5. Only 4 of 27 USPCBs are deep fill-out factors ($f > 50\,\%$). And 16 of 27 systems are shallow contact ($f < 20\,\%$). Unlike the F and G type contact binaries, non of their mass ratios are less than 0.3. Generally, shallow contact factor implies an early phase of contact. According to the thermal relaxation oscillation (TRO) theory (Lucy 1976; Flannery 1976; Webbink 1977), the material flow started when the primary component (donor) fully filled its Roche lobe, which made the orbit shrinking, and then, the secondary component (accretor) fully filled its Roche lobe, too. The accretor will expand continuously when it accepted masses, which made the orbit wider, until the contact configuration broke. Subsequently, the orbit will shrink again with the mass transfer from the primary to the secondary component. It forms a cycle of contact-semidetached-contact. In these cycles, the temperatures of the two components will be similar because of a thermal exchange with the mass transfer, and the fill-out fact cannot reach high when a system undergoes the TRO cycle because of the existence of the contact broken phase. Hence, TRO explained why it is such high fraction

of shallow USPCBs (16 of 27 systems). And for this reason, the zero contact binary within thermal equilibrium, 1SWASP J030749.87−365201.7, should be in the turn-off phase of the TRO cycle. On the other hand, however, the TRO theory cannot explain the presence of the deep USPCBs with high or moderate mass ratios (e.g., 1SWASP J200059.78+054408.9).

If the USPCBs would reach a deep fill-out factor, a rapid orbit shrinking mechanism is required. Angular momentum loss (AML) caused by the magnetic stellar winds (e.g. Stępień 2006, 2011) may be the mechanism. He pointed out that if there is a third body or the system is located in a dense field, it can lose a lot of AM. An excessive AML also can occurred in the pre-main-sequence phase. In that time, he said these possibilities, especially for the last one, are quite rare, according to the observations (Stępień 2006). However, some studies showed that the third bodies is not very rare (e.g., Pribulla & Rucinski 2006; D'Angelo et al. 2006; Rucinski et al. 2007; Qian et al. 2013b, 2015b). Maybe the few deep USPCBs in Table 5, including 1SWASP J200059.78+054408.9, are formed by the rare AML way, e.g., interaction with third bodies.

5. Global parameter correction of the ultrashort-period contact binaries

The physical parameters of close binaries are sufficiently different from the singles or wide binaries because of the strong inter-gravity. For example, the surface gravity accelerations of components in contact binaries systems are observably less than those of the same masses single main-sequence stars. Hence, to obtain these parameters for close binaries independently is very important to build an improved evolutionary model for them. The USPCBs are predicted that they have a well empirical global parameter relation than that of F, G and early K type contact binaries because most of them are near the zero age main sequence and unevolved. This character is good for estimating the parameters of USPCBs when it lacks of spectroscopic data. Dimitrov & Kjurkchieva (2015) had already summarized a relationship between the period and the semi-major axis, based on the 14 well-studied binaries with P < 0.27 d ($a = -1.154 + 14.633 \times P - 10.319 \times P^2$). However, one point deviated this relation, i.e., GSC 1387-0475. It was first investigated by Rucinski & Pribulla (2008) with yielding a spectroscopic mass ratio. Nevertheless, their photometric light curve was not quality well. Yang et al. (2010) observed this system again and obtained a BVR-bands light curve. They adopted the spectroscopic mass ratio yielded by Rucinski & Pribulla (2008), and found smaller masses of the components than the results of the former. We assumed that the inconformity of these two results is caused by the deep fill-out factor. Consequently, we realized that the semi-major axis probably is over estimated with the relation of Dimitrov & Kjurkchieva (2015) when the fill-out factor is huge (e.g. $f > 50\,\%$). According to the well

known Roche potential,

$$\psi = \frac{2}{1+q} \cdot \frac{1}{r_1} + \frac{2q}{1+q} \cdot \frac{1}{r_2} + (x - \frac{q}{1+q})^2 + y^2 \tag{1}$$

where ${r_1}^2 = x^2+y^2+z^2$, ${r_2}^2 = (1-x)^2+y^2+z^2$, $q = M_2/M_1$, xyz are normalized coordinates (with semi-major axis, A), and with the definition of fill-out factor

$$f = \frac{\psi - \psi_{\rm in}}{\psi_{\rm out} - \psi_{\rm in}}, \tag{2}$$

we compute the $r_{\rm side}$, $r_{\rm back}$ and $r_{\rm pole}$ with a certain fill-out factor f and mass ratio q. The effective radius is calculated by $r_{\rm E} = \sqrt[3]{r_{\rm side} \cdot r_{\rm back} \cdot r_{\rm pole}}$. Then, we compare this $r_{\rm E}$ to $r_{\rm L}$ which was yielded by Eggleton (1983) with an error less than 1 %,

$$r_{\rm L} = \frac{0.49 q^{-2/3}}{0.6 q^{-2/3} + \ln(1 + q^{-1/3})}. \tag{3}$$

Finally, we obtain a ratio of these two normalized radii, and use it to correct the semi-major axis. The corresponding results are list in Table 6. All errors in this table are estimated with the error propagation formula. We find that the masses of GSC 1387-0475 are high close to the values of Yang et al. (2010) after the correction. We adopt the corrections to 1SWASP J200059.78+054408.9. It may be composed by two M type components with mass $0.458 \pm 0.066\,M_\odot$ and $0.199 \pm 0.033\,M_\odot$, respectively.

6. Conclusions

1SWASP J030749.87−365201.7 is a zero contact binary, with $q = 0.439 \pm 0.003$ and $f = 0.0 \pm 3.6$ %. It is on the turn-off phase of the TRO cycle. 1SWASP J213252.93−441822.6 is a shallow contact binary with $q = 0.560 \pm 0.003$ and $f = 14.2 \pm 1.9$ %. It is under the TRO controlling. 1SWASP J200059.78+054408.9 is a deep contact binary, with $q = 0.436 \pm 0.008$ and $f = 58.4 \pm 1.8$ %. It should be formed by a rapid AML mechanism. All targets showed strong magnetic activities. In summary, 1SWASP J030749.87−365201.7 and 1SWASP J200059.78+054408.9 are in particular evolutionary stages. They are worth to monitor in future.

We thank Allen W. Shafter for giving us constructive suggestions that improved the paper greatly.

This work is partly supported by the Yunnan Natural Science Foundation (2016FB004), the young academic and technology leaders project of Yunnan Province (No. 2015HB098),

Chinese Natural Science Foundation (Nos. 11403095 and 11325315), the Key Research Programme of the Chinese Academy of Sciences (grant No. KGZD-EW-603), and Strategic Priority Research Programme "The Emergence of Cosmological Structures" of the Chinese Academy of Sciences (No.XDB09010202). New observations of the two south sky targets were obtained with the 2.15m telescope at Complejo Astronómico El Leoncito observatory (CASLEO), San Juan, Argentina, and those of the north sky target were obtained with the 1.88 m Kottamia reflector telescope in Egypt.

REFERENCES

Barnes, J. R., & Collier Cameron, A. 2001, MNRAS, 326, 950

Barnes, J. R., James, D. J., & Cameron, A. C. 2004, MNRAS, 352, 589

Barnes, J. R., Jeffers, S. V., Jones, H. R. A., Pavlenko, Ya. V., Jenkins, J. S., Haswell, C. A., Lohr, M. E. 2015, ApJ, 812, 42

Becker, A. C., Bochanski, J. J., Hawley, S. L., et al. 2011, ApJ, 731, 17

Claret, A., and Gimenez, A., 1990, A&A 230, 412

Cutri, R. M. et al. 2003, yCat, 2246, 0

D'Angelo, C., van Kerkwijk, M. H., Rucinski, S. M. 2006, AJ, 132, 650

Davenport, J. R. A., Becker, A. C., West, A. A. 2013, ApJ, 764, 62

Dimitrov D. P. & Kjurkchieva D. P. 2015, MNRAS, 448, 2890

Djurasevic G., Yilmaz M., Basturk O., Kilicoglu T., Latkovic O., Caliskan S. 2011, A&A, 525, 66

Eggleton, P. P. 1983, ApJ, 268, 368.

Elkhateeb, M. M., Saad, S. M., Nouh, M. I., & Shokry, A. 2014a, NewA, 28, 85

Elkhateeb, M. M., Nouh, M. I., Saad, S. M., & Zaid, I. 2014b, NewA, 32, 10

Essam, A., Djurašević, G., Ahmed, N. M., & Jurković, M. 2014, NewA, 32, 16

Flannery, B. P. 1976, ApJ, 205, 217

Jiang L.-Q., Qian S.-B., Zhang J. and Zhou X. 2015a, AJ, 149, 169

Jiang L., Qian S.-B. and Zhang J. 2015b, RAA, 15, 2237

Jiang L.-Q., Qian S.-B., Zhu L.-Y., Zhang J. and Zhou X. 2015c, NewA, 41, 22

Jiang L., Qian S.-B., Zhang J. and Liu N. 2015d, PASJ, 67, 118

Köse O., Kalomeni B., Keskin V., Ulaş B. and Yakut K. 2011, AN, 332, 626K

Koen C., Koen T., Gray R. O. 2016, AJ, 151, 168

Koen, C. 2014, MNRAS, 441, 3075

Liu, L., Chen, W. P., Qian, S. B., et al. 2015a, AJ, 149, 111

Liu, N.-P., Qian, S.-B., Soonthornthum, B., Zhu, L.-Y., Liao, W.-P., Zhao, E.-G., Zhou, X. 2015b, AJ, 149, 148

Lohr, M. E., Norton, A. J., Kolb, U. C., et al. 2013, A&A, 549, A86

Lohr, M. E., Norton, A. J., Kolb, U. C., & Boyd, D. R. S. 2013, A&A, 558, A71

Lohr, M. E., Hodgkin, S. T., Norton, A. J., & Kolb, U. C. 2014, A&A, 563, A34

Lucy, L. B., 1967, Zeitschrift für

Lucy, L. B. 1976, ApJ, 205, 208

Maceroni, C., & van't Veer, F. 1996, A&A, 311, 523

Mullan, D. J. 1975, ApJ, 198, 563

Norton, A. J., Payne, S. G., Evans, T., et al. 2011, A&A, 528, A90

O'Connell, D. J. K. 1951, Publications of the Riverview College Observatory, 2, 85

Paczyński, B., Szczygieł, D. M., Pilecki, B., & Pojmański, G. 2006, MNRAS, 368, 1311

Pribulla, T., Rucinski, S. M. 2006, AJ, 131, 2986

Qian, S.-B., Liu, L., Zhu, L.-Y., He, J.-J., Yang, Y.-G., Bernasconi, L. 2011, AJ, 141, 151

Qian, S.-B., Liu, N.-P., Li, K. et al. 2013a, ApJS, 209, 13

Qian, S.-B., Zhang, J., Wang, J.-J. et al. 2013b, ApJS, 207, 22

Qian, S. B., Zhang, B., Soonthornthum, B. et al. 2015a, AJ, 150, 117

Qian, S.-B., Jiang, L.-Q., Fernández Lajús, E. et al. 2015b, ApJ, 798L, 42

Rucinski, S. M., & Pribulla, T. 2008, MNRAS, 388, 1831

Rucinski, S. M., Pribulla, T., van Kerkwijk, M. H. 2007, AJ, 134, 2353

Rucinski, S. M., 1969, A&A 19, 245

Rucinski, S. M. 1992, AJ, 103, 960

Rucinski, S. M. 1997, MNRAS, 382, 393

Samec, R. G., Faulkner, D. R., Williams, D. B. 2004, AJ, 128, 2997

Stępień, K. & Gazeas, K. 2012, AcA, 62, 153

Stępień K. 2006, AcA, 56, 199

Stępień K. 2011, AcA, 61, 139

Tout, C. A., & Hall, D. S. 1991, MNRAS, 253, 9

Webbink, R. F. 1977, ApJ, 211, 881

Wilson, R. E., & Devinney, E. J. 1971, ApJ, 166, 605

Wilson, R. E., & van Hamme, W. 2014, ApJ, 780, 151

Wilson, R. E., Van Hamme, W., & Terrell, D. 2010, ApJ, 723, 1469

Wilson, R. E. 1979, ApJ, 234, 1054

Wilson, R. E. 1990, ApJ, 356, 613

Wilson, R. E. 2008, ApJ, 672, 575

Wilson, R. E. 2012, AJ, 144, 73

Worthey, G., & Lee, H.-C. 2011, ApJS, 193, 1

Yang, Y.-G., Wei, J.-Y., Li, H.-L. 2010, NewA, 15, 155

B. Zhang, S. B. Qian, Z. Miloslav, L. Y. Zhu, N. P. Liu, 2017, NewA, 54, 52

Van Hamme, W., & Wilson, R. E. 2007, ApJ, 661, 1129

Table 1: Summary of the observations.

Target	Obs Date	Texp (s)	Filter	N Img	Telescope	Seeing (″)
1SWASP J030749.87−365201.7	2014-11-24	30	I	471	2.15 m JST	3.0-7.0
	2014-11-25	30	I	440	2.15 m JST	3.5-7.5
	2014-12-03	30	V	669	2.15 m JST	3.5-7.5
	2014-12-04	60	B	325	2.15 m JST	3.5-7.0
1SWASP J213252.93−441822.6	2015-09-11	60	R	308	2.15 m JST	3.4-7.4
1SWASP J200059.78+054408.9	2016-08-01	200	V	49	1.88 m KRT	3.0-6.5
	2016-08-01	135	R	46	1.88 m KRT	3.0-6.5
	2016-08-01	170	I	46	1.88 m KRT	3.0-6.5

Table 2: The JHK magnitudes for the targets, comparisons and check stars. Estimated temperatures of the primary components for the three USPCBs based on the JHK colours.

Name	J (mag)	H (mag)	K (mag)	J-K	Type	T_p (K)
1SWASP J030749.87−365201.7	13.552	13.007	12.887	0.665	Target	4750
2MASS J03075380−3653319	12.840	12.407	12.359	0.481	Comparison	
2MASS J03075601−3652174	15.165	14.910	14.873	0.292	Check	
1SWASP J213252.93−441822.6	14.299	13.667	13.622	0.677	Target	4700
2MASS J21325995−4418032	12.782	12.317	12.228	0.554	Comparison	
2MASS J21330002−4418197	13.652	13.263	13.178	0.474	Check	
1SWASP J200059.78+054408.9	13.412	12.875	12.764	0.648	Target	4800
2MASS J20011488+0543026	13.519	13.162	13.048	0.471	Comparison	
2MASS J20011491+0542524	13.420	13.204	13.225	0.195	Check	

Table 3: Photometric solutions for the three USPCBs.

	1SWASP J030749.87−365201.7		1SWASP J213252.93−441822.6		1SWASP J200059.78+054408.9	
Parameters	Photometric elements	errors	Photometric elements	errors	Photometric elements	errors
$g_1 = g_2$	0.32	assumed	0.32	assumed	0.32	assumed
$A_1 = A_2$	0.50	assumed	0.50	assumed	0.50	assumed
$x_{1bolo} = x_{2bolo}$	0.315	assumed	0.315	assumed	0.311	assumed
$y_{1bolo} = y_{2bolo}$	0.371	assumed	0.370	assumed	0.377	assumed
$x_{1V} = x_{2B}$	1.036	assumed	–	–	–	–
$y_{1V} = y_{2B}$	−0.216	assumed	–	–	–	–
$x_{1V} = x_{2V}$	0.682	assumed	–	–	0.658	assumed
$y_{1V} = y_{2V}$	0.135	assumed	–	–	0.162	assumed
$x_{1R} = x_{2R}$	0.423	assumed	0.437	assumed	0.407	assumed
$y_{1R} = y_{2R}$	0.343	assumed	0.330	assumed	0.360	assumed
$x_{1I} = x_{2I}$	0.258	assumed	–	–	0.247	assumed
$y_{1I} = y_{2I}$	0.423	assumed	–	–	0.433	assumed
Phase shift	–	–	–	–	0.0032	±0.0006
T_h (K)	4750	±700	4700	±400	4800	±300
T_c (K)	4697	±703	4671	±405	4528	±316
$q = M_c/M_h$	2.280	±0.010	1.785	±0.007	2.296	±0.040
Ω_{in}	5.6432	–	4.9443	–	6.4432	–
Ω_{out}	5.0383	–	4.3545	–	5.8264	–
$\Omega_1 = \Omega_2$	5.6431	±0.0220	2.0763	±0.0033	5.3123	±0.0112
$i(^\circ)$	78.2	±0.1	81.9	±0.1	75.3	±0.5
$L_1/(L_1+L_2)(B)$	0.3415	±0.0015	–	–	–	–
$L_1/(L_1+L_2)(V)$	0.3231	±0.0012	–	–	0.4196	±0.0067
$L_1/(L_1+L_2)(R)$	0.3035	±0.0010	0.3789	±0.0013	0.3975	±0.0054
$L_1/(L_1+L_2)(I)$	0.2801	±0.0009	–	–	0.3850	±0.0048
$r_1(pole)$	0.2951	±0.0014	0.3165	±0.0012	0.3200	±0.0064
$r_1(side)$	0.3079	±0.0017	0.3319	±0.0015	0.3392	±0.0082
$r_2(back)$	0.3402	±0.0027	0.3692	±0.0025	0.4027	±0.0195
$r_2(pole)$	0.4185	±0.0013	0.4124	±0.0011	0.4547	±0.0049
$r_2(side)$	0.4449	±0.0016	0.4386	±0.0014	0.4924	±0.0069
$r_2(back)$	0.4724	±0.0021	0.4704	±0.0020	0.5333	±0.0102
f (%)	0.0	±3.6	14.2	±1.9	58.4	±1.8

Table 4: Cool spot elements based on the light curve solutions.

		θ (°)	ψ (°)	Ω(sr)	T_s/T_*
1SWASP J030749.87−365201.7	star 1	89.95	157.08	0.35845	0.700
	star 2	86.51	235.49	0.22845	0.850
	star 2	89.95	180.00	0.27845	0.700
1SWASP J213252.93−441822.6	star 2	89.67	77.01	0.20800	0.700
1SWASP J200059.78+054408.9	star 2	89.70	134.30	0.20845	0.700

Table 5: 27 well-studied USPCBs.

Name	Period (day)	$q = M_s/M_p$	$f(\%)$	$i(^\circ)$	M_p^*	M_s^*	R_p^*	R_s^*	reference
1SWASP J030749.87−365201.7	0.2266712	0.439	0.0	78.2	0.789	0.346	0.737	0.507	This paper
RW Com	0.2373464	0.471	6.1	74.9	0.849	0.400	0.774	0.549	Djurasevic et al. (2011)
NSVS 2700153	0.228456	0.775	7.1	47.8	0.650	0.504	0.662	0.589	Dimitrov & Kjurkchieva (2015)
1SWASP J055416.98+442534.0	0.21825	0.792	8.6	70.1	0.582	0.461	0.618	0.556	Dimitrov & Kjurkchieva (2015)
1SWASP J200503.05−343726.5	0.2288836	0.934	9.0	73.8	0.599	0.560	0.637	0.617	Zhang et al. (2017)
1SWASP J160156.04+202821.6	0.22653	0.670	10.0	79.5	0.679	0.455	0.675	0.563	Lohr et al. (2014); Essam et al. (2014)
1SWASP J022727.03+115641.7	0.21095	0.463	10.4		0.659	0.305	0.658	0.464	Liu et al. (2015a)
1SWASP J150822.80−054236.9	0.23006	0.514	12.0	90.0	0.774	0.398	0.729	0.538	Lohr et al. (2014)
1SWASP J074658.62+224448.5	0.22085	0.395	12.6	78.6	0.769	0.304	0.726	0.476	Jiang et al. (2015a)
1SWASP J080150.03+471433.8	0.217531	0.432	13.6	83.8	0.723	0.313	0.698	0.476	Dimitrov & Kjurkchieva (2015)
1SWASP J213252.93−441822.6	0.22123459	0.560	14.2	81.9	0.690	0.386	0.679	0.521	This paper
1SWASP J015100.23−100524.2	0.2145001	0.320	14.6	79.4	0.760	0.243	0.724	0.432	Qian et al. (2015b)
V1104 Her	0.22788	0.623	15.0		0.707	0.441	0.692	0.557	Liu et al. (2015b)
CC Com	0.22068516	0.526	17.0	89.8	0.701	0.369	0.685	0.511	Köse et al. (2011)
SDSS J012119.10C001949.9	0.2052	0.500	18.9	83.9	0.600	0.300	0.622	0.454	Jiang et al. (2015b)
NSVS 7179685	0.20974	0.451	19.3	85.5	0.655	0.295	0.656	0.457	Dimitrov & Kjurkchieva (2015)
NSVS 8626028	0.217407	0.805	20.7	65.9	0.573	0.461	0.612	0.555	Dimitrov & Kjurkchieva (2015)
2MASS J00164102−0009251	0.198561	0.630	22.0	53.3	0.507	0.319	0.564	0.457	Davenport et al. (2013)
1SWASP J024148.62+372848.3	0.21975076	0.813	23.3	68.7	0.585	0.475	0.621	0.565	Jiang et al. (2015c)
1SWASP J133105.91+121538.0	0.21801	0.828	25.2	77.6	0.570	0.472	0.611	0.561	Elkhateeb et al. (2014a)
V523 Cas	0.233693	0.516	29.0	85.4	0.798	0.412	0.744	0.550	Samec et al. (2004)
1SWASP J210318.76+021002.2	0.22859	0.877	34.2	81.9	0.616	0.540	0.645	0.607	Elkhateeb et al. (2014b)
1SWASP J200059.78+054408.9	0.20569054	0.435	58.4	75.3	0.631	0.274	0.642	0.439	This paper
NSVS 925605	0.217629	0.678	70.2	57.2	0.618	0.419	0.637	0.533	Dimitrov & Kjurkchieva (2015)
GSC 1387−0475	0.21781128	0.474	76.3	49.9	0.705	0.334	0.687	0.489	Yang et al. (2010)
1SWASP J075102.16+342405.3	0.20917224	0.740	96.0	76.0	0.543	0.401	0.590	0.514	Jiang et al. (2015d)
1SWASP J234401.81−212229.1	0.21367	0.422		79.4	0.699	0.295	0.683	0.461	Lohr et al. (2013b); Koen (2014)

* Computed by the relation of Dimitrov & Kjurkchieva (2015) and by eqution 3. The footnote P denotes the primary component, while S denotes the secondary component.

Table 6: Semi-major axis corrections for the deep USPCBs.

Name	1SWASP J200059.78+054408.9	NSVS 925605	GSC 1387−0475	1SWASP J075102.16+342405.3
Period (day)	0.20569054	0.21762900	0.21781128	0.20917224
$q = M_s/M_p$	0.436 ± 0.008	0.678 ± 0.003	0.474 ± 0.008	0.740 ± 0.040
$f(\%)$	58.4 ± 1.8	70.2 ± 2.6	76.3 ± 2.9	95.0 ± 4.0
Refrence	This paper	Dimitrov & Kjurkchieva (2015)	Yang et al. (2010)	Jiang et al. (2015d)
a $(R_\odot)$	1.419 ± 0.050	1.542 ± 0.050	1.544 ± 0.050	1.455 ± 0.050
$r_{\rm L1}$	0.452 ± 0.005	0.413 ± 0.004	0.445 ± 0.004	0.405 ± 0.004
$r_{\rm L2}$	0.310 ± 0.003	0.346 ± 0.003	0.316 ± 0.003	0.353 ± 0.004
$r_{\rm E1}$	0.492 ± 0.011	0.475 ± 0.012	0.502 ± 0.012	0.505 ± 0.012
$r_{\rm E2}$	0.352 ± 0.010	0.412 ± 0.010	0.380 ± 0.011	0.467 ± 0.011
$cor = (r_{\rm L1}/r_{\rm E1} + r_{\rm L2}/r_{\rm E2})/2$	0.899 ± 0.013	0.854 ± 0.013	0.860 ± 0.015	0.780 ± 0.010
$a' = a \cdot cor(R_\odot)$	1.276 ± 0.064	1.317 ± 0.063	1.327 ± 0.066	1.135 ± 0.054
$M_p(M_\odot)$	0.458 ± 0.066	0.385 ± 0.055	0.448 ± 0.064	0.257 ± 0.031
$M_s(M_\odot)$	0.199 ± 0.033	0.261 ± 0.038	0.212 ± 0.034	0.190 ± 0.033
$R_p = r_{\rm E1} \cdot a'(R_\odot)$	0.628 ± 0.046	0.626 ± 0.046	0.666 ± 0.049	0.572 ± 0.041
$R_s = r_{\rm E2} \cdot a'(R_\odot)$	0.449 ± 0.035	0.543 ± 0.039	0.504 ± 0.040	0.530 ± 0.038

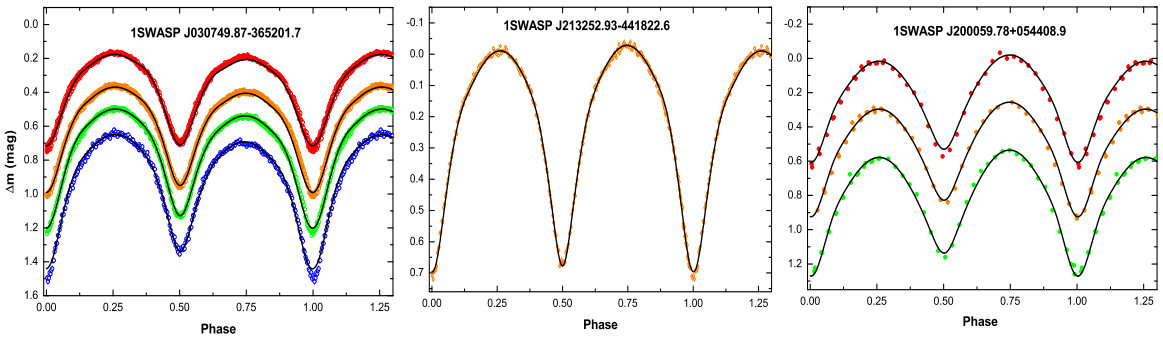

Fig. 1.— Observed and fitted curves for the three USPCBs. The colour points denote the observed data with different filters. Blue denotes B filter; green denotes V filter; orange denotes R filter; red denotes I filter. The black solid lines are the theoretical fittings, with the modeling of dark spots.

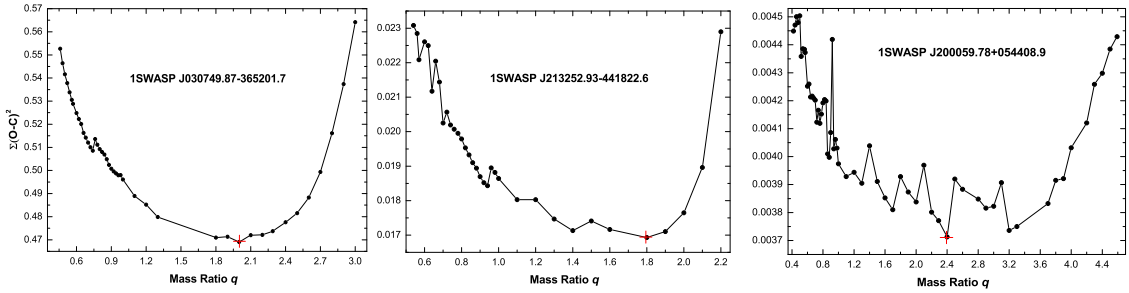

Fig. 2.— The relation between q and fitting residuals for the three USPCBs. The red cross in each diagram presents the initial value of q at the beginning of the W-D program running.

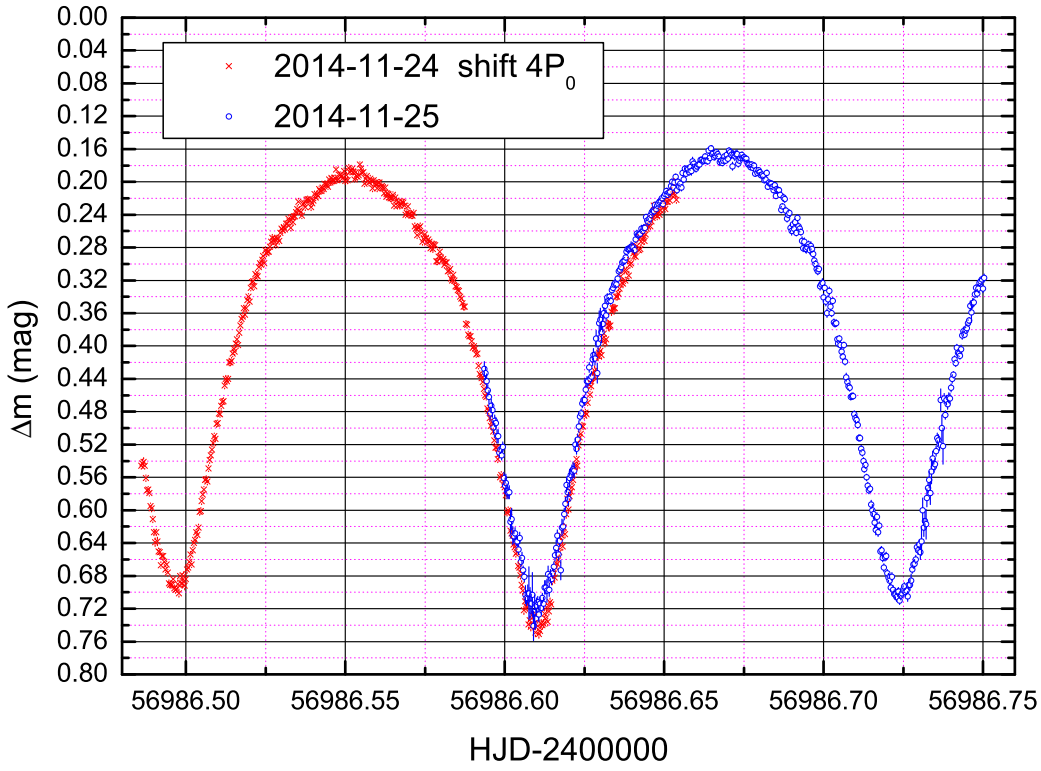

Fig. 3.— The night-to-night light curve variation of 1SWASP J030749.87−365201.7. The red data points were observed on the night of 2014-11-24 with the I filter, while the blue data points were observed on the night of 2014-11-25 with the same filter. We add four times of P_0 (0.2266712 day) to the red points. However, this two parts of light curves do not join well. Moreover, a changing of depths of minima is clear seen. This phenomenon could be caused by variations of the presented cool spots.

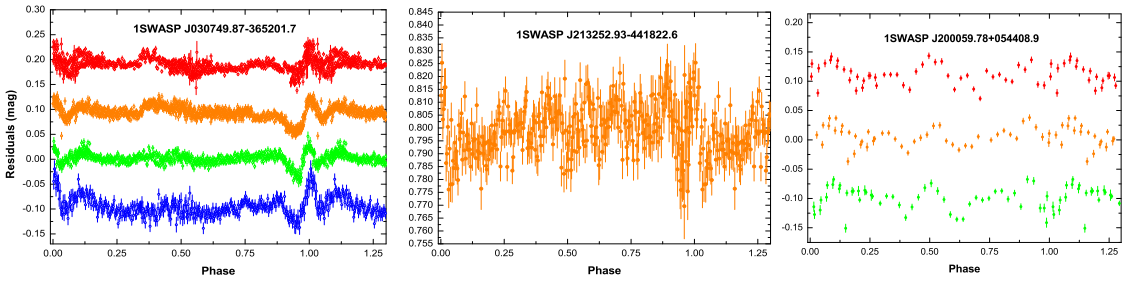

Fig. 4.— Fitting residuals of light curves for the three USPCBs. The colours denote the same meaning as the Fig 1.

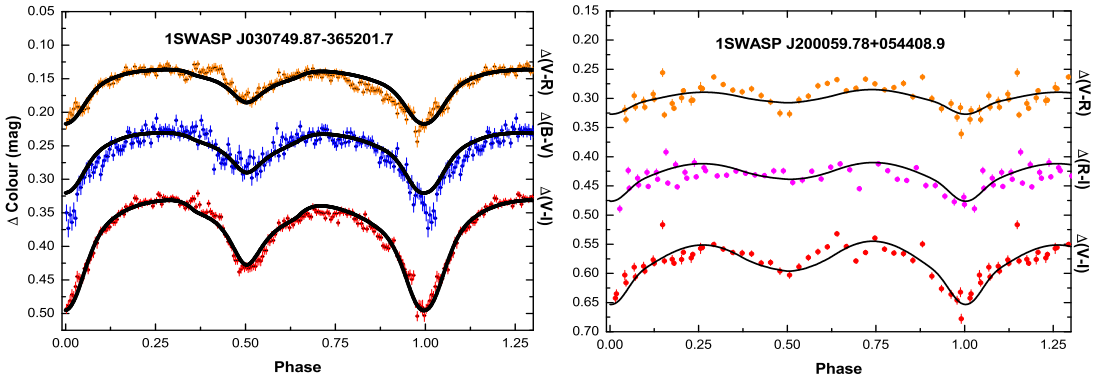

Fig. 5.— Observed differential colours for the three USPCBs. Blue denotes Δ(B-V); orange denotes Δ(V-R); red denotes Δ(V-I); magenta denotes Δ(R-I). The solid lines are yielded by the W-D program.

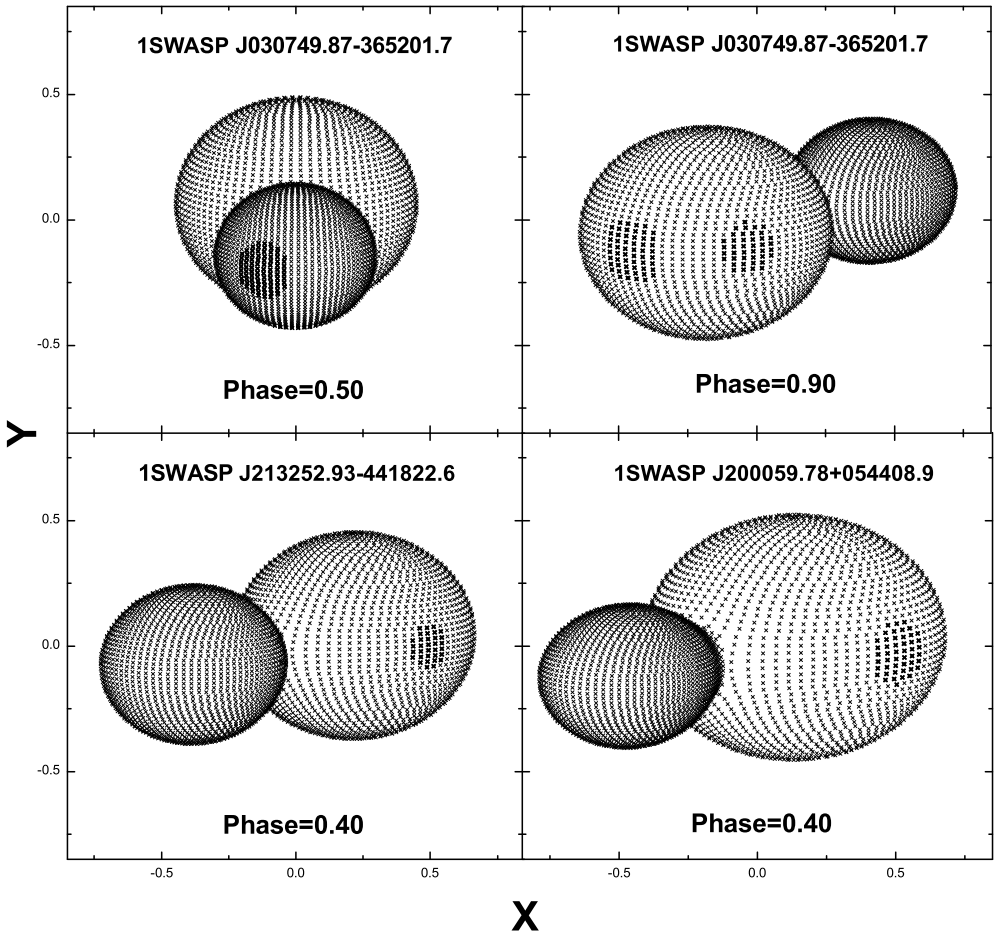

Fig. 6.— The geometrical structure of the three USPCBs with their present cool spots.